Southern Illinois University Edwardsville

SPARK

SIUE Faculty Research, Scholarship, and Creative Activity

2018

Electrochemical investigation of the kinetics of chloride substitution upon reduction of [Ru(porphyrin)(NO)Cl] complexes in THF.

Jeremy R. Zink
University of Oklahoma Norman Campus, jzink@ou.edu

E G. Abucayon
University of Oklahoma

Anthony R. Ramuglia
Southern Illinois University Edwardsville, aramugl@siue.edu

Arghavan Fadamin
SIUE

James E. Eilers
Southern Illinois University Edwardsville, jeilers@siue.edu

See next page for additional authors

Follow this and additional works at: https://spark.siue.edu/siue_fac

Part of the Inorganic Chemistry Commons

Recommended Citation

Zink, Jeremy R.; Abucayon, E G.; Ramuglia, Anthony R.; Fadamin, Arghavan; Eilers, James E.; Richter-Addo, George B.; and Shaw, Michael J., "Electrochemical investigation of the kinetics of chloride substitution upon reduction of [Ru(porphyrin)(NO)Cl] complexes in THF." (2018). *SIUE Faculty Research, Scholarship, and Creative Activity*. 74.
https://spark.siue.edu/siue_fac/74

This Article is brought to you for free and open access by SPARK. It has been accepted for inclusion in SIUE Faculty Research, Scholarship, and Creative Activity by an authorized administrator of SPARK. For more information, please contact jkohlbu@siue.edu.

Authors

Jeremy R. Zink, E G. Abucayon, Anthony R. Ramuglia, Arghavan Fadamin, James E. Eilers, George B. Richter-Addo, and Michael J. Shaw

This article is available at SPARK: https://spark.siue.edu/siue_fac/74

Electrochemical investigation of the kinetics of chloride substitution upon reduction of [Ru(porphyrin)(NO)Cl] complexes in THF.

Jeremy R. Zink,[a,b] Erwin G. Abucayon,[b] Anthony R. Ramuglia,[a] Arghavan Fadamin,[a] James E. Eilers,[a] George B. Richter-Addo,[b] and Michael J. Shaw,*[a]

Dedicated to Professor Alan Bond on the occasion of his 70th birthday.

Abstract: The electrochemistry of several ruthenium porphyrin nitrosyl chloride complexes [Ru(por)(NO)Cl] have been examined in tetrahydrofuran. The complexes undergo 1-electron irreversible reductions which result in the diffusion-limited substitutions of the chloride ligands for THF. This chloride metathesis is reversible in the presence of added NBu_4Cl, and equilibrium constants and rate constants for chloride loss have been estimated. These parameters correlate with the NO stretching frequencies of the parent complexes, with more electron-donating porphyrin ligands favouring chloride loss from the reduced complexes. The [Ru(por)(NO)(THF)] products of the reductions can be detected by IR, EPR and visible spectroscopies. These species undergo three further reductions, with good reversibility at scan rates >0.40 V s^{-1}. The $[Ru(por)(NO)(THF)]^{+/0}$ couples have also been determined, and the rate constants and equilibrium constants for recombination with chloride have been estimated. One-electron reductions of the [Ru(por)(NO)Cl] complexes result in ~10^{18} enhancement of the rates of chloride loss.

Introduction

[M(porphyrin)NO]-containing species (M = Fe, Ru, Os) have been investigated by us[1] and others[2-5] as models for heme-NO interactions.[6, 7] The redox behavior of model complexes of the heme-NO systems continue to be of interest, especially with regard to the chemical transformation of the NO ligand. Six-coordinate $[Fe(porphyrin)(NO)L]^+$ (L = 2-electron neutral donor such as 5-methylimidazole) models are important since various redox states have been shown or implicated in the reactivity of these species.[7,8]

The site of electron-transfer in such complexes can be either the porphyrin ligand or the M-NO unit, and the complexes have the potential to be either 5-coordinate or 6-coordinate. Most ferrous [Fe(porphyrin)NO] complexes possess square pyramidal geometry with a bent NO ligand, i.e. $\{FeNO\}^7$ in Enemark-Feltham notation[9] where the "7" indicates the total number of electrons in the metal's d-orbitals (with NO excluded) and the π* orbitals of the NO ligand. A smaller number of 6-coordinate Fe(III) species such as [Fe(porphyrin)(NO)(X)] and $[Fe(porphyrin)(NO)(L)]^+$ (X = 1-electron anionic donor) have been structurally characterized.[1a-c,10,11] The congeneric Ru systems such as [Ru(porphyrin)(NO)(X)] (X = halide, alkoxide, thiolate, alkyl, aryl) have been explored as models for their Fe analogues.[12] To date, structurally well-characterized examples of [Ru(porphyrin)(NO)] species appear to be exclusively 6-coordinate, regardless of the $\{RuNO\}^n$ (n = 6, 7) count.[7]

The difference between 5-coordination and 6-coordination can have a profound effect on the outcome of the reactions of [Fe(porphryin)(NO)] species. We recently reported that treatment of a stable 6-coordinate $[Fe(OEP)(NO)(MeIm)]^+$ complex (OEP = octaethylporphyrin, MeIm = 5-methylimidazole) with hydride yields a bound HNO ligand (an important and biologically relevant species)[13]) whereas the reaction of 5-coordinate $[Fe(OEP)(NO)]^+$ complex with hydride yields an Fe-hydride species, presumably by direct attack at the accessible metal center.[1a,11e] An implication is that 6-coordination can be strategy for protection of the metal-center during reactions that modify the NO ligand.

Electrooxidation of [Ru(porphyrin)(NO)X] species is well-established, and often results in porphyrin-based π-radical cation complexes.[1d, 14] Previous studies of a number of [Ru(porphyrin)(NO)Cl] compounds in CH_2Cl_2 have been reported.[14d,f] These studies reveal that the porphyrin complexes undergo two reversible oxidation processes. The reductions of these compounds in CH_2Cl_2 are less straightforward, however. They show poor reversibility by cyclic voltammetry (CV) methods, with broad return waves upon scan reversal, and appear to be multi-electron based on comparison of the observed currents to the oxidation feature in the same scan.

While CH_2Cl_2 is an attractive solvent for these studies, there are drawbacks to its use. [Fe(porphyrin)Cl] studies by Saveant show that reductions can lead to reaction with halogenated hydrocarbons.[15] For example, 2-electron reduction of [Fe(TPP)Cl] (TPP = *meso*-tetraphenylporphyrin) in the presence of CH_3I leads to the formation of the $[Fe(TPP)CH_3]$ complex at the electrode surface.[16] Another problem with CH_2Cl_2 as a solvent is that it can participate in halogen-atom abstraction

[a] A. R. Ramuglia, A. Fadamin, Dr. J. E. Eilers, Dr. M. J. Shaw, Department of Chemistry
Southern Illinois University Edwardsville
Box 1652, Edwardsville, Illinois, USA 62026
E-mail: michsha@siue.edu:

[b] J. R. Zink, Dr. E.G Abucayon, Dr. G.B. Richter-Addo
Department of Chemistry and Biochemistry
University of Oklahoma
101 Stephenson Parkway, Norman, Oklahoma USA 73019.

Supporting information for this article is given via a link at the end of the document.

WILEY-VCH

reactions.[17] Tetrahydrofuran (THF) is often a better solvent for the study of reductions, as it has a wide voltammetric window for reduction and can be rendered rigorously dry by distillation from an alkali metal. While THF can occasionally serve as an H-atom source, given the weak C-H bond in the 2-position, [18] such activity is rare. It is noted that THF has a relatively limited solvent window for the study of oxidations. Kaim et al. characterized a $\{RuNO\}^7$ complex, [Ru(TTP)(NO)(pyridine)], by spectroscopic and computational means.[14f] Kadish and Richter-Addo reported a related electrochemically-generated [Ru(TPP)(NO)(pyridine)] species.[14a] As a Lewis base, THF is expected to stabilize coordinatively unsaturated species better than CH_2Cl_2.

The difficulty in characterizing the reduction processes for [Ru(porphyrin)(NO)X] complexes has limited their utility as model compounds for iron-heme NO species, especially for the biologically-important $\{FeNO\}^7$ state. In this paper, the consequences of reduction of [Ru(por)(NO)X] in THF are established (por = TAP, TTP, T(*p*-Cl)PP, OEP, where TAP = *meso*-tetra(*p*-OCH_3)phenylporphyrin, TTP = *meso*-tetra(*p*-CH_3)phenylporphyrin, T(*p*-Cl)PP = *meso*-tetra(*p*-Cl)phenylporphyrin, OEP = octaethylporphyrin). Specifically, estimates of thermodynamic parameters (*E°'* values and equilibrium constants) and kinetic parameters (i.e., rate constants) for post-electron-transfer reactions are determined.

Results and Discussion

Overview: As described in detail below, the consequences of the reduction of the [Ru(por)(NO)Cl] species in THF include bending of the NO ligand and diffusion-controlled replacement of a chloride ligand for a solvent molecule as shown in Eq. 1 and 2 where "Ru" = [Ru(por)(NO)]. The thus-formed neutral solvento-species has a rich redox chemistry summarized in Eq. 3-6.

$[RuCl]^0 + e^- \leftrightarrows [RuCl]^-$ $\quad E°'(RuCl)$ (1)

$[RuCl]^- + THF \leftrightarrows [Ru(THF)]^0 + Cl^-$ $\quad K_1, k_{f1}$ (2)

$[Ru(THF)]^0 + e^- \leftrightarrows [Ru(THF)]^-$ $\quad E°'(Ru^{0/-1})$ (3)

$[Ru(THF)]^- + e^- \leftrightarrows [Ru(THF)]^{2-}$ $\quad E°'(Ru^{-1/-2})$ (4)

$[Ru(THF)]^{2-} + e^- \leftrightarrows [Ru(THF)]^{3-}$ $\quad E°'(Ru^{-2/-3})$ (5)

$[Ru(THF)]^+ + e^- \leftrightarrows [Ru(THF)]^0$ $\quad E°'(Ru^{+1/0})$ (6)

Digital simulations of CV data yield rate and equilibrium data for Eq. 2. In the presence of added chloride, the rate and equilibrium constants for recombination of Cl^- with $[Ru(por)(NO)(THF)]^+$ (Eq. 7) can be determined.

$[Ru(THF)]^+ + Cl^- \leftrightarrows [RuCl]^0$ $\quad K_2, k_{f2}$ (7)

The kinetic and thermodynamic parameters reasonably correlated with the electron density at the metal center as determined by the v(NO) values. Finally, there is indication for the TAP and OEP species of a competing reaction which we propose includes the formation of a diruthenium species.

Method of CV Data Analysis

Many inorganic chemists do not take full advantage of the wealth of information available by CV because of a hesitancy to use iR_u compensation during data collection. This work relies on accurate measures of how CV peak potentials change with scan rates, and we sought to use the opportunity to test whether data correction methods which rely on the correction of an internal standard[19] could rival the results obtained with iR_u compensated data. We found very satisfactory agreement.

The effects of iR_u-drop complicate reliable extraction of kinetic parameters from CV data.[20] Publishable data with minimal iR_u-drop is usually collected with iR_u-compensation applied by the potentiostat during data collection.[21] In this work, data was collected both with and without *iR*-compensation applied, so that post-data collection correction techniques could be compared with results from iR_u-compensated data for the same system. As described in the literature, Eq. 8 and 9[22,23] can be used to correct Faradaic currents for iR_u-drop and charging current. Values of uncompensated resistance (R_u) can be estimated from the slope of an Ohm's law plot of E_{pa} vs. i_{pa} of the $[(C_5Me_5)_2Fe]$ internal standard. The capacitance (C_{dl}) is extracted from the charging current in background scans.

$$E'(t) = E(t) + R_u \cdot i(t) \qquad (8)$$

In Eq. 8, $E'(t)$ is the corrected experimental potential (in V) recorded at a specific time, t (in s), $E(t)$ is the uncorrected experimental potential (in V) at a specific time, and $i(t)$ is the experimental currents (in A). In Eq. 9, $i_f(t)$ is the Faradaic current (in A) and R_u is the uncompensated resistance (in Ω).

$$i_f(t) = i(t) - C_{dl}\frac{dE'(t)}{dt} + C_{dl}R_u\frac{d\,i(t)}{dt} \qquad (9)$$

The data in this work is presented in dimensionless format to show clearly how the shapes of the voltammograms change as scan rate is varied. Eq. 10 describes how current, $i(t)$, is transformed into its dimensionless format, $\psi(t)$. [20b, 23]

$$\psi(t) = \frac{i(t)}{FAc\sqrt{\frac{DF\nu}{RT}}} \qquad (10)$$

In Eq. 10, F = 96485.3 C mol^{-1}, A = electrode surface area (cm^2), c = concentration (mol cm^{-3}), D = diffusion coefficient (cm^2 s^{-1}), v = scan rate (V s^{-1}), R = 8.31441 J mol^{-1} K^{-1}, and T = temperature (K). The $[(C_5Me_5)_2Fe]^{+/0}$ feature used as an internal standard in every scan is not expected to show the theoretical 0.446 height for a 1-electron transfer[20b, 23] in plots where the focus is on the Ru-complexes since its values of c and D are different from the [Ru(por)(NO)Cl] complexes. The D values of 4 x 10^{-6} cm^2 s^{-1} for the Ru complexes gave self-consistent results although this value is at the lower end of the range expected. The value measured by

WILEY-VCH

chronoamperometry for [Ru(OEP)(NO)Cl] in CH_2Cl_2 for its reversible 1-electron oxidation was D = 8 x 10^{-6} cm^2 s^{-1}, and correction with the Stokes-Einstein relation as described in ref [24] for the difference in solvent viscosity yields a value of D = 7 x 10^{-6} cm^2 s^{-1}, but this value does not take into account differences in coordination, polarity, and ion-pairing, all of which might be expected to lower the diffusion coefficient.

The peak potentials determined from iR_u-corrected CV data compare favorably with iR-compensated data. To further explore the nuances of this approach, we compared the effect of the data processing methods on simple control systems and on DigiElch simulations of data which included or excluded R_u and C_{dl}. This work is described in detail in the supplementary information (Figs. S1-S5, Tables S1 and S2). Briefly, for a 0.1M NBu_4PF_6 solution which contains both 1.0 mM [Cp_2Fe] and 1.0 mM [Cp_2Co]BF_4 (Cp = η^5-C_5H_5), correction of the [Cp_2Fe] feature at each scan rate so that its ΔE_p value became 59 mV also corrects the cobaltocenium feature's ΔE_p value to 58-61 mV (Fig. S2) and yields overlapping convolved plots for this feature (Fig. S3). This result was also obtained on data simulated with DigiElch (Fig. S4). For simulations of EC mechanisms similar to that proposed herein for the Ru porphyrin systems, the corrected data also yielded potentials very close to the "ideal" expected in the absence of resistance and capacitance (Fig. S5).

Surprisingly, the currents observed for both methods show similar distortions; i.e., dimensionless plots of data did not overlap perfectly for the internal standard but showed a dependence on scan rate (supplementary Fig. S6). The data corrected with Eqs. 8 and 9 are expected to have problems with the magnitude of the currents, since the correction process essentially has the same effect as decreasing the scan rate at high currents, but it was surprising (to us) that this effect was also present in iR-compensated data (supplementary Fig. S6).

Conveniently, the distortions in the dimensionless peak currents can be corrected by comparison with an internal standard present in the same scan as discussed in the supplementary material (Tables S2). Although we did not require such correction for this work, the procedure is simple and might be of value in situations where existing data was collected without iR-compensation.

A final method used to present and compare CV data in this work was convolution, as described by Bard and Faulkner, and by Saveant.[21, 22, 23] The transformation of dimensionless CV data with Eq. 11 results in a plot similar to a polarogram, where the y-axis represents equivalents of electrons transferred.

$$I(t) = \frac{1}{\sqrt{\pi}} \int_0^t \frac{i(u)}{\sqrt{t-u}}\, du \qquad (11)$$

In Eq. 11, $I(t)$ represents the "convolved" current, $i(u)$ represents the current measured at position u during the voltammogram. LabView 2012 software was written (MJS) using Bard and Faulkner's algorithm for evaluating this integral for digitized data.[25]

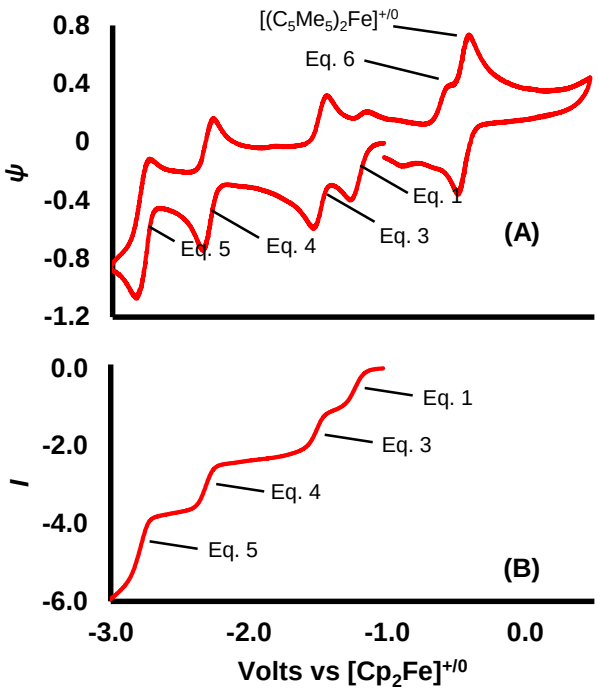

Figure 1. (A) Dimensionless-current representation of CV data for 1.5 mM [Ru(TAP)(NO)Cl] in 0.1M NBu_4PF_6/THF at 0.20 V/s at 298 K. Forward features are labelled with the redox processes discussed in the text. (B) Convolved plot of first data segment of data in (A).

Cyclic voltammetry of [Ru(por)(NO)Cl] species

Fig. 1A shows iR_u-compensated CV data for 1.5 mM [Ru(TAP)(NO)Cl] in 0.1M NBu_4PF_6/THF at 298 K in the presence of 1.0 mM [$(C_5Me_5)_2Fe$]. All of the [Ru(por)(NO)Cl] species in this work display similar voltammetry data, with differences in potential owing to the different electron-donating abilities of the various porphyrin ligands. The TPP complex was not soluble enough in THF to give meaningful quantitative results. Although its features appear qualitatively consistent with the other four complexes, it will not be discussed further. The $E°'$ values of the observed features, as obtained from digital simulations (see below) are summarized in Table 1 along with ν(NO) values for each complex. Figure 1B shows the convolved data (Eq. 11) from Fig. 1A. Since all the features have similar plateau heights they represent similar numbers of electrons transferred, i.e. about 1-electron in height, if the D-value is accurate. Each complex has a feature at ca -1.0 to -1.2 V vs $Cp_2Fe^{+/0}$ which is chemically irreversible at scan rates of 0.05 – 1.6 V/s and when the scan is reversed at potentials slightly more negative than the peak potential. A small return peak is sometimes visible when subsequent reduction features are scanned. In the presence of 10 mM added chloride, this feature shows improved chemical

Table 1. *E°'* values (V vs $[Cp_2Fe]^{+/0}$) of features observed in voltammograms of [Ru(por)(NO)Cl] complexes in THF.

Redox Process	TAP	TTP	T(p-Cl)PP	OEP
$[RuCl]^{0/-}$	-1.51	-1.53	-1.47	-1.60
$[Ru(THF)]^{+/0}$	-0.60	-0.60	-0.54	-0.73
$[Ru(THF)]^{0/-1}$	-1.47	-1.48	-1.43	-1.55
$[Ru(THF)]^{-1/-2}$	-2.33	-2.36	-2.22	-2.47
$[Ru(THF)]^{-2/-3}$	-2.79	-2.88	-2.67	-3.01

reversibility especially at slow scan rates. This behavior indicates that reversible loss of chloride (Eq. 2) is the chemical step which follows electron-transfer.

At the right of Fig. 2, the internal standard $[(C_5Me_5)_2Fe]^{+/0}$ is visible, as well as a shoulder due to a reversible feature assigned to the oxidation of $[Ru(TTP)(NO)(THF)]^0$ (Eq. 6) to its cationic form. The latter feature is not visible unless the reduction feature is scanned first, and it is present when no internal standard is added, so this feature is not an artifact of interaction with $[(C_5Me_5)_2Fe]$. The size of this peak and the extent of its reversibility are affected by the addition of chloride, presumably because of recombination of the $[Ru(por)(NO)(THF)]^+$ cation with Cl^- (Eq. 7). This observation allows for the determination of the K_2 and k_{f2} values for the recombination reaction listed in Eq. 7 through simulation and curve-fitting. Eq. 7 completes a thermodynamic cycle with Eq. 1, 2, and 6, so K_2 is not an independent variable and can be calculated using Eq. 12. Comparison of data and simulations (see below) for the OEP, TAP, and T(*p*-Cl)PP complexes are shown in Figs S7-S12.

$$K_2 = \frac{1}{K_1} e^{\left\{\frac{nF(E^{o'}(RuCl) - E^{o'}(Ru^{+/0})}{RT}\right\}} \qquad (12)$$

The dimensionless-current data in Figure 2 is corrected with Eq. 8 and 9 so that the ΔE_p values for the $[(C_5Me_5)_2Fe]^{+/0}$ internal standard (*E°'(THF)* = -0.449 V vs. $Cp_2Fe^{0/+}$)[26], visible at right of Figures 1 and 2, is approximately 59 mV, as expected from theory.[27] The resulting changes in the shape of the [Ru(por)(NO)Cl] reduction features upon chloride addition are consistent with Saveant's zone diagram for an EC reaction.[23] The shape of the wave (Fig. 2A) starts in the purely kinetic (KP) zone where the feature is irreversible. Upon addition of chloride, there is improved reversibility (Fig. 2B) of the reduction but with a broad return wave, consistent with the system's movement into the equilibrium/kinetic zone (KE). These observations indicate that the follow-up chemical reaction is not only fast, but that the chemical step in this EC mechanism is a reversible, fast equilibrium reaction. The addition of chloride eliminates the shoulder on the internal standard attributed to Eq. 7.

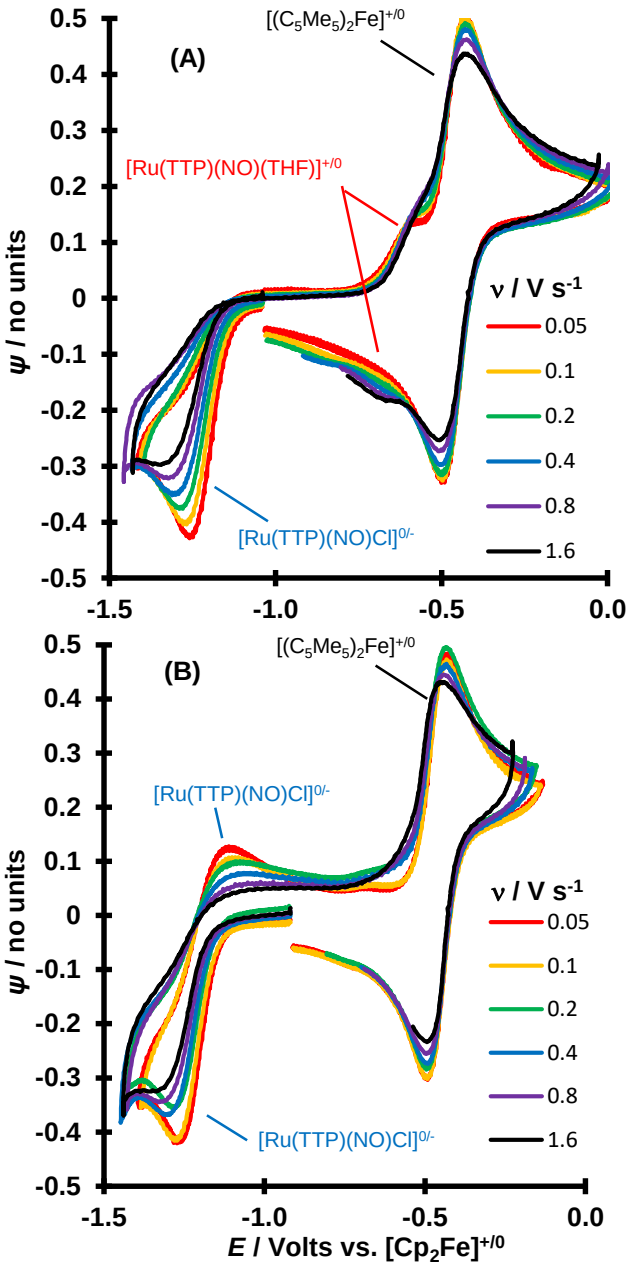

Figure 2. (A) Dimensionless-current CV plots of 1.6 mM Ru(TTP)(NO)Cl in 0.1M NBu_4PF_6/THF at 298K, data corrected as per Eq. 8 and 9, and (B) with 10 mM NBu_4Cl.

The slope of a plot of E_{pc} vs log(v) is diagnostic of whether the electron-transfer step or chemical step is rate-limiting.[28] A slope of -29.6 mV indicates that the chemical step is rate- limiting, whereas a slope of 59.2 mV indicates that the chemical step is concerted with electron-transfer, or at least occurs at the diffusion rate limit. This analysis requires that iR_u drop be eliminated from data for the results to be trustworthy, hence our emphasis on checking the quality of the data correction methods.

Table 2. Slopes of $\delta E_{pc}/\delta\log(v)$ (mV) plots [for Ru(por)(NO)Cl] complexes' first reduction feature.

por	$\delta E_{pc}/\delta\log(v)$[a]	$\delta E_{pc}/\delta\log(v)$[b]
1.5mM OEP	-56.9	-63.3
0.5 mM TAP:	-46.0	[c]
1.6 mM TTP	-60.8	-62.6
0.6 mM T(p-Cl)PP	-57.2	-57.2

[a] Data collected with iR compensation. [b] data collected without iR compensation, and corrected as described in the text. [c] Not available.

The observed slopes for the [Ru(por)(NO)Cl] compounds fall in the narrow range of -56.9 to -63.3 mV, as listed in Table 2, with the TAP complex being the only outlier at -46.0 mV. The conclusion is that the reversible chemical step in Eq. 2 occurs at the solvent-diffusion limited rate, which can be calculated to be 1.34×10^{10} M^{-1} s^{-1} from the viscosity of THF.[29] The establishment of this rate allows for digital simulations to find *E°'* values and the equilibrium constants for Eq. 1 and 2 through curve fitting as described below. The slopes for data collected with *iR*-compensation are close enough to the values obtained from corrected data to validate the use of these methods in this work.

At potentials more negative than -2 V vs. $[Cp_2Fe]^{+/0}$, two more reduction features are visible in Fig. 1A. The latter two reduction features are likely to be porphyrin-based, and cannot be observed in CH_2Cl_2 as they lie beyond its solvent limit. These features correspond to the processes in Eq. 4 and 5, and we propose that they are porphyrin-based processes, based on features observed for complexes of non-redox active metals.[30] The feature labelled Eq. 4, i.e. the $Ru^{-/2-}$ couple, shows good chemical reversibility at all scan rates used. In rigorously dry solvent, the feature labelled Eq. 5, i.e. the $Ru^{2-/3-}$ couple, shows reversibility at scan rates higher than 400 mV/s with plateau behavior for some compounds at lower scan rates. Since the potential of this final feature is very negative it is not surprising that it is sensitive to trace moisture. The potentials for this process are listed in Table 1 and range from about -2.8 to -3.0 V vs $[Cp_2Fe]^{+/0}$, values which are not dissimilar to the potentials required to reduce alkali metal cations.[31]

Finally, for the OEP and TAP complexes, a new peak was observed as a shoulder on the $E°'(Ru(THF)^{0/-1})$ process (i.e. the second reduction feature) after chloride addition. Careful examination of the lowest scan rate voltammograms for the OEP complex showed hints of this feature in the absence of added chloride. This observation, and the observation of an extra band in the IR spectroelectrochemistry (see below) suggests the analysis of the $[Ru(OEP)(NO)Cl]^0$ complex might be more complicated than the other complexes.

Concentration studies were undertaken to determine whether second-order reactions make a significant contribution to the observed electrochemistry. For each complex, CV data was collected at three different concentration ranges, specifically 0.15 - 0.25 mM, 0.9 - 1.1 mM, and 1.5 - 1.6 mM. Dimensionless-current representations for the TTP complex as a representative example are shown in supplementary Fig. S13. The shapes of the waves are very similar on forward scans, although the data do not overlay perfectly for the first two reduction features. However, the feature for the $E°'(Ru(THF)^{-/2-})$ matches very well. The concentration-dependence of the peak heights is indicative of a contribution of a reaction that is second-order in ruthenium, but that all species converge towards the $[Ru(por)(NO)(THF)]^-$ form at more negative potentials and/or longer timescales. The effect of the [Ru(por)(NO)Cl] concentration on the voltammograms thus limits the accuracy in the parameters found from simulation of Eq. 1.- Eq. 7. (Table 4, below). However, the error is expected to be small since the overall rate of dimerization must be slow with respect to chloride substitution because of the low concentrations of the [Ru(por)(NO)Cl] complexes, even if dimerization has a large rate constant.

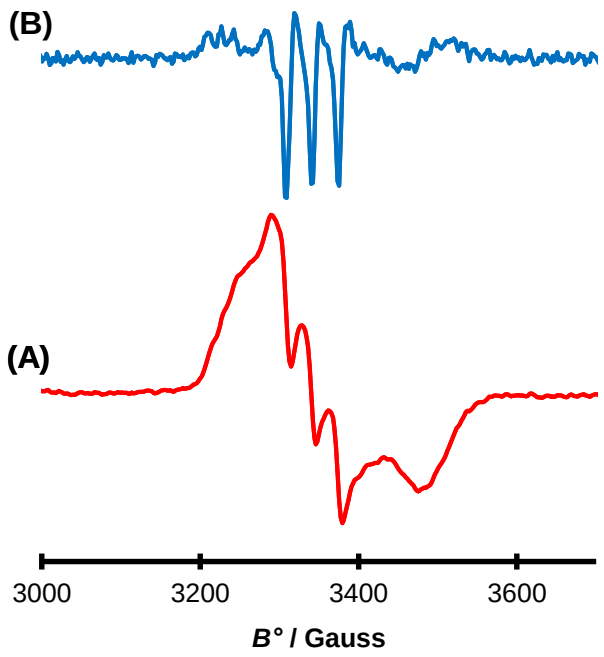

Figure 3. (A) Anisotropic EPR spectrum of [Ru(OEP)(NO)(THF)] recorded at 77 K in 0.1M NBu_4PF_6/THF, 1st derivative plot (B) 2nd Derivative plot showing $\alpha(^{14}N)$ splitting of high-field component.

EPR Spectroscopy

The [Ru(OEP)(NO)Cl] complex was reduced by 1 electron with excess cobaltocene in 0.1 M NBu_4PF_6/THF in an inert-atmosphere drybox under argon. The supporting electrolyte is added so that conditions match those used for CV studies, and to improve the formation of an amorphous glass at 77 K. Under the conditions used in our laboratories at SIUE, *E°'* for $[Cp_2Co]$ in NBu_4PF_6/THF at 298 K is measured to be -1.31 V vs. $[Cp_2Fe]^{+/0}$. This potential is reducing enough to cause the first, irreversible

reduction of [Ru(OEP)(NO)Cl] to occur but is insufficiently negative to reduce the neutral [Ru(OEP)(NO)(THF)] product. A yellowish precipitate is observed in these reactions, which is presumably $[Cp_2Co]Cl$.

The isotropic EPR spectrum recorded at 298 K displays a broad featureless singlet for this solution. However, the isotropic spectrum recorded at 77K (Fig. 3A) displays typical features for a 6-coordinate $\{RuNO\}^7$ complex, using Enemark-Feltham notation.[32] The observed spectral parameters (g_1 = 2.036, g_2 = 1.985 ($\alpha(^{14}N)$ = 33 G), g_3=1.880) compare very well with literature values from Kaim's work for the [Ru(TPP)(NO)(pyridine)] complex (g_1 = 2.054 ($\alpha(^{14}N)$ = 17 G), g_2 = 1.985 ($\alpha(^{14}N)$ = 33 G), g_3=1.908).[14f] Specifically, the small separation in g-values is in contrast to the large separation in g-values observed for Ru(III) complexes.[33] Fig. 3B shows the second derivative plot of the EPR data, which shows that the high-field feature is split into a 1:1:1 triplet with $\alpha(^{14}N)$ = 17 G. This splitting is not always observable for $\{RuNO\}^7$ complexes, but is typical of values in the literature when the feature is observed. Almost identical spectra were obtained when the experiment was repeated in the presence of excess NBu_4Cl as a chloride source.

Spectroelectrochemistry

The changes in *v*(NO) were investigated by fiber-optic IR spectroelectrochemistry. The OEP and TAP derivatives have been previously studied by this method in CH_2Cl_2, and the new results are consistent with previous observations.[14d] In this method, an IR beam is brought to an electrode at a 90° angle. It passes through a thin layer of solution, reflects from the electrode and passes through the solution again. Background IR data is recorded at a potential at which current does not flow, and a sample spectrum is then recorded while the electrode potential is set to a value slightly more negative than the peak potential of interest. This geometry minimizes the contributions to the final difference spectrum of surface-bound species, since there is a node (i.e., zero intensity) in the IR-beam at the reflective surface. The method is most sensitive to species in the diffusion layer, since IR bands which do not change in intensity (i.e., from the bulk solution) do not appear in the final difference spectrum.[34] The timescale of data collection by this method is comparable to the CV timescale, but determination of reversibility by this method is not quantitative since the bulk solution is not electrolyzed.

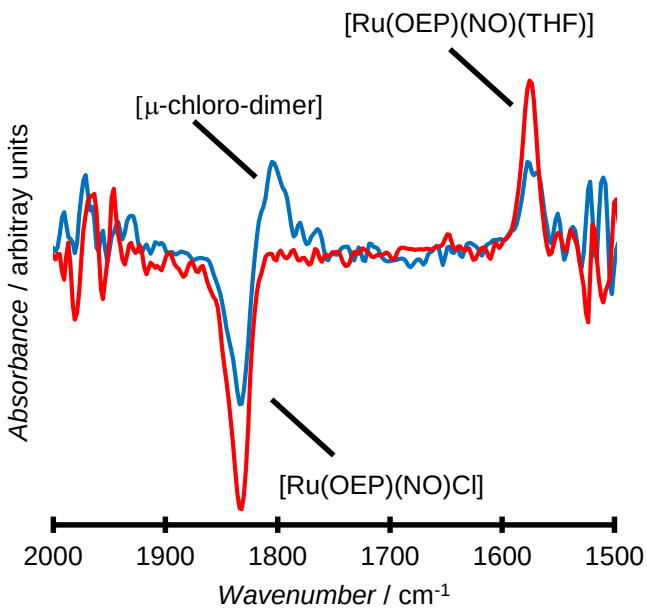

Figure 4. IR spectroelectrochemistry of [Ru(OEP)(NO)Cl] in 0.1 M NBu_4PF_6/THF at 298 K, Blue: $E_{applied}$ = -1.4 V vs. $[Cp_2Fe]^{+/0}$, Red: $E_{applied}$ = -1.6 V vs $[Cp_2Fe]^{+/0}$.

Upon reduction of [Ru(por)(NO)Cl] at a potential slightly more negative than the first reduction feature, the intensity of the v(NO) band (1833-1844 cm^{-1}) decreases and a new band appears in the 1576-1584 cm^{-1} range, i.e., some 300 cm^{-1} lower in frequency. This change is consistent with the transformation of a linear Ru-NO unit in the starting material to a bent Ru-NO unit in the product. This new band is assigned to the neutral $[Ru(por)(NO)(THF)]^0$ species. The v(NO) frequencies of the observed features are listed in Table 3.

These features appear more intense when the electrode potential is set slightly more negative than the second reduction feature. The IR bands of the supporting electrolyte and THF obscure the region where the v(NO) band for the $[Ru(por)(NO)(THF)]^-$ anion is expected to appear. However, the peak in the 1576-1584 cm^{-1} range also increases in intensity, since the $[Ru(por)(NO)(THF)]^-$ anion is stable and reducing enough to react with [Ru(por)(NO)(Cl)] to produce more $[Ru(por)(NO)(THF)]^0$.

For the OEP derivative, a second v(NO)band at 1801 cm^{-1} is clearly visible when a fresh electrode is used (Figure 4). It is unlikely that the band at 1801 cm^{-1} corresponds to the $[Ru(OEP)(NO)Cl]^-$ species. This band is putatively assigned to an intermediate di-Ru species $[(Ru(OEP)(NO))_2(\mu\text{-}Cl)]^-$, as discussed below, and is consistent with the observation of concentration dependence in the CV data. The band is visible in subsequent scans, but less intense. This band is only 31 cm^{-1} lower in frequency than the band for the starting material, and it clearly remains in the frequency range for a linear Ru-NO unit. Even without bending, a change of >80 cm^{-1} would be expected for a M-NO-centered redox process.[12] It is unlikely that the Ru-NO unit is the site of electron transfer for the species that gives rise to this band. The oxidations of the [Ru(OEP)(NO)Cl] complex in CH_2Cl_2 have been established as porphyrin-centered processes, and changes in v(NO) of 30 cm^{-1} are observed.[14d] Closer examination of the data for the other porphyrin complexes in this study indicates that a very weak band with similar shifts from the starting material is visible in data when a fresh electrode is used, as indicated in Table 3.

DFT calculations on anionic $[Ru(porphyrin)(NO)Cl]^-$ indicate a bent Ru-NO unit (143° calculated), for which the v(NO) value should be some 300 cm^{-1} lower than the starting material, with a weak Ru-Cl bond (2.48 Å). A comparison of selected calculated structural parameters between the neutral and anionic forms is shown in supplementary Table S3. Figures S14-S16 show the total electron density, the LUMO of the neutral form, and

the HOMO of the anionic form respectively. Addition of Cl^- to the solution does not change the observed spectra significantly. The lability of the chloride ligand in this species would result in a very small concentration of $[Ru(porphyrin)(NO)Cl]^-$ at an electrode surface even in the presence of added Cl^-.

Table 3. Changes in IR bands observed by fiber-optic IR spectroelectrochemistry for Ru(por)(NO)Cl in 0.1M NBu_4PF_6 / THF at 298 K.

Porphyrin Complex	v(NO) in THF cm^{-1}	v(NO) changes, 1st reduction	v(NO) changes, 2nd reduction
OEP	1833	↓1833 ↑1803(s), 1576	↓1834 ↑1576
TAP	1893	↓1839 ↑1807(w), 1580	↓1839 ↑1580
TTP	1840	↓1840 ↑1810(vw), 1582	↓1840 ↑1582
T(p-Cl)PP	1844	↓1833 ↑1803(s), 1576	↓1844 ↑1585

For [Ru(OEP)(NO)Cl], VIS-NIR spectroelectrochemistry was performed. No spectral changes were observed in the 900 – 1750 nm region upon application of potential. In the 400-900 nm region, reduction of [Ru(OEP)(NO)Cl] in 0.1M NBu_4PF_6 / THF at 298 K at a potential slightly negative of its first reduction led to increases in intensity at 539 nm and 574 nm which reached steady state after 2 minutes. This behavior is very similar to that observed by Kaim for the reduction of $[Ru(OEP)(NO)(pyridine)]^+$, where a similar pattern of peaks at 524 and 577 nm increased in intensity upon reduction.[14f] Thus, the reduction is consistent with the formation of neutral [Ru(OEP)(NO)(THF)].

Reduction at a potential slightly negative of the second reduction led to more intense features at 539 and 574 nm, and a shoulder at 522 nm. After addition of excess chloride, bands at the same wavelengths were observed as in the absence of chloride for the first reduction. On the other hand, addition of chloride caused the band at 522 nm to increase substantially relative to the features at 544 and 573 nm when the electrode potential was set past the second reduction. We note that the $[Ru(OEP)(MeCN)_2]$[35] and $[Ru(OEP)(O\text{-}DMSO)_2]$ complexes have been reported, and the latter has a band at 520 nm in its VIS spectrum,[36] and the $[Ru(OEP)(THF)_2]$ species which would result from NO loss might be reasonably expected to show a similar feature. Thus, it is possible that the presence of chloride accelerates the loss of NO from the Ru complex, as has been observed for analogous iron complexes.[11b]

Digital Simulation and Curve Fitting of CV data

Fig. 5 shows a representative example of the fit between experimental and simulated CV data for [Ru(TTP)(NO)Cl] in THF. Representative overlaid plots at multiple scan rates for the compounds in this study are found as Figures S17-S25. Fig. 6 shows optimized curve-fitted simulations for [Ru(TTP)(NO)Cl] using Eqs. 1-7 as a mechanism, displayed as

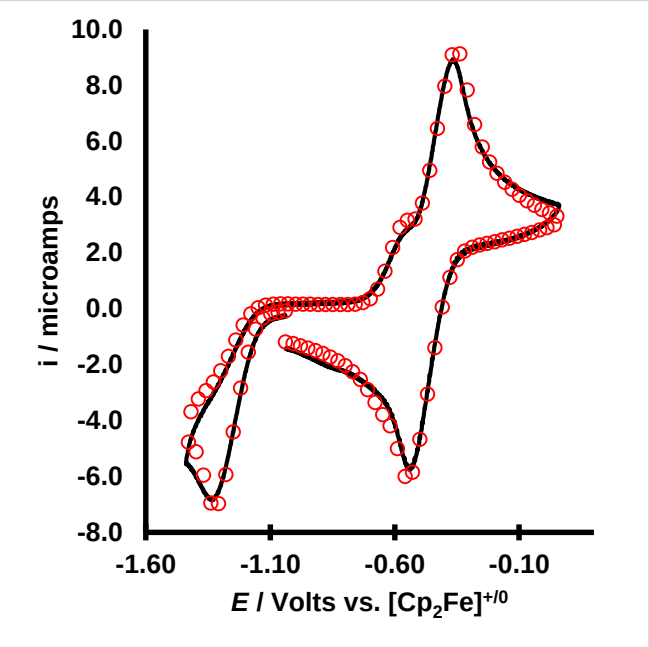

Figure 5. (A) Overlay of simulations (O) and experimental (—) CV trace for 1.6 mM [Ru(TTP)(NO)Cl] in 0.1 M NBu_4PF_6/THF at 298K at 0.2 V s^{-1}, parameters as in Tables 1 and 4.

iR-corrected dimensionless plots. Comparison with Fig. 2 shows excellent agreement between the two sets, although the simulations systematically overestimate the peak currents of the $[Ru(por)(NO)(THF)]^{+/0}$ couple (for all porphyrins) when excess chloride is added. Uncorrected experimental data collected without iR_u compensation was used for these simulations and values of R_u and C_{dl} determined from the data set were included in the simulation mechanism. The simulated data are displayed in dimensionless-current format with the same corrections for R_u and C_{dl} applied as for the experimental data shown in Fig. 2 so that side-by-side evaluation of the changes in CV shape may be made. The parameters found for the four porphyrin complexes are shown in Table 4.

General guidelines for CV curve fitting have been discussed in the literature,[37] and specific considerations of the curve fitting process in this work are described in the Experimental section. Consistent with these guidelines, many parameters are available by inspection of the available experimental data. These include the $E°'$ values for reversible CV features, the value of k_{f1} deduced from the slope E_{pc} vs. log(v) plots, and values from thermodynamic cycles, e.g. K_2. Initial values for $E°'(RuCl)$ for Eq. 1 were evaluated from intercepts of plots of E_{pc} vs ln(v) according to Eq. 13, assuming k_{f1} is diffusion limited. [Equation 2.6 in ref. 35].

$$E_p = E° - 0.78\frac{RT}{F} + \frac{RT}{2F}\ln\left(\frac{RTk_f}{Fv}\right) \qquad (13)$$

Surprisingly, the $E°'(RuCl)$ values obtained in this way were slightly more negative than the observed values for $E°'(Ru(THF)^{0/-1})$ values, and did not change appreciably when curve fitting was used to optimize their values. The exceedingly

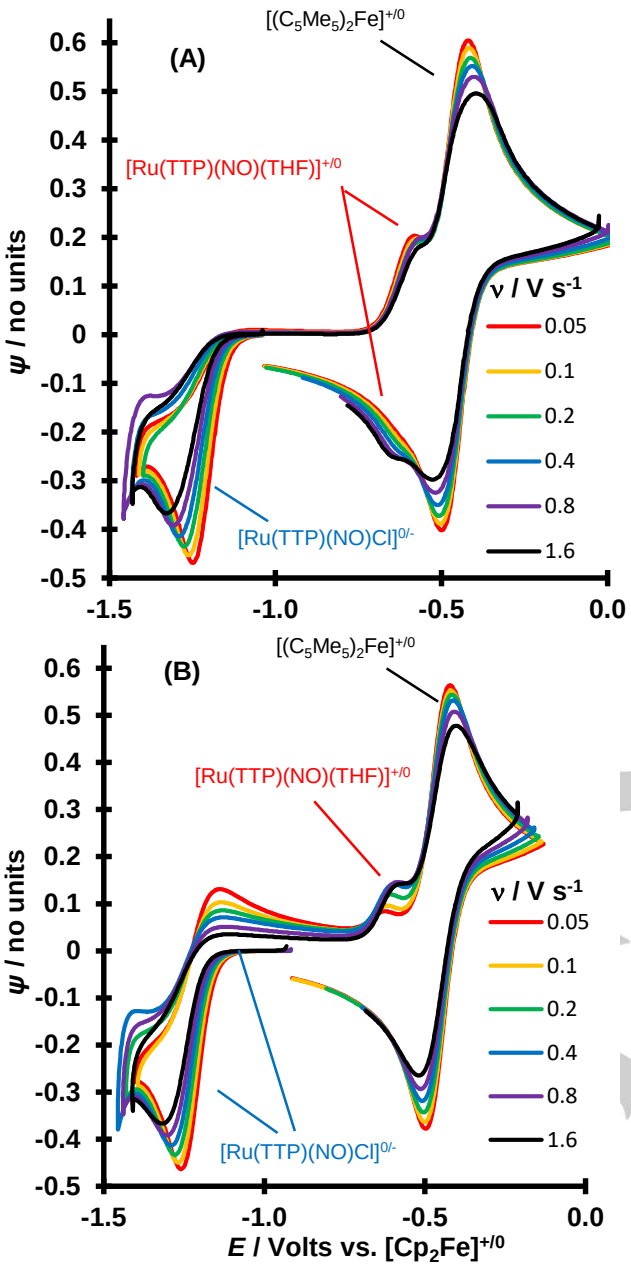

Figure 6. (A) Simulations of 1.6 mM [Ru(TTP)(NO)Cl] in 0.1 M NBu_4PF_6/THF at 298K, parameters as in Tables 1 and 4. (B) Simulations which include includes 10 mM chloride.

fast follow-up reaction moves the observed irreversible reduction feature to more positive potentials. This stabilization is not observed in CH_2Cl_2, where the first two redox features seem to coincide, most likely for lack of a good Lewis base to occupy the site *trans* to the NO ligand. Clear changes in CV shape result from the addition of chloride, and the only unknown value which contributes to this process is K_1. Thus, the value of K_1 found by curve-fitting should be a robust measure of the tendency for the [Ru(por)(NO)Cl]$^-$ anion to undergo chloride-for-solvent exchange.

The values obtained for K_2 and k_{f2} also appear to be robust. For each complex, these parameters routinely refine to the final values shown in Table 4, even when starting with widely divergent starting values. In addition, final K_2 and k_{f2} values appeared to be independent of the specific values chosen for k_{f1} and $E°'(RuCl)$, as long as the latter two variables are consistent with Saveant's Equation 2.6 from reference [23], and K_1 is large enough to prevent the first reduction from appearing reversible. The result is that the equilibrium constants and the rate constants for chloride replacement by THF for the various [Ru(por)(NO)Cl]$^{0/-}$ complexes can be reliably compared.

The set of four [Ru(por)(NO)Cl] compounds used in this work have ν(NO) values which span a range of only 11 cm^{-1}, but this range corresponds to changes in redox potentials of ca. 0.1-0.25 V, as apparent in Table 1. The $E°'$ values for the various electron-transfer reactions are plotted against the ν(NO) values in Figure S26. Linear relationships are found, with the most electron-rich complexes being the most difficult to reduce. This result indicates a linear free energy relationship between the amount of electron density on the metal center in the starting material, and the redox properties of each pertinent species in Eq. 1-7. These plots have R^2 values about 0.97 except for $E°'(Ru(THF)^{2-/3-})$, for which R^2 = 0.90, most likely due to the uncertainty in the measurement of the OEP complex because of plateau currents which we attribute to reaction with adventitious moisture. The measured potential (-3.00 V vs $Cp_2Fe]^{0/+}$) rivals that of the reduction of sodium ions.[31] It is gratifying that the results for

Table 4. Equilibrium (K) and rate (k_f and k_r) constants for the EC process for the reversible loss of Cl from various [Ru(por)(NO)Cl] species..

Porphyrin Complex	Eq.	K	k_f M^{-1} s^{-1}	k_r [a] M^{-1} s^{-1}
OEP	2	1.6 x 10^3	1.3 x 10^{10} [b]	8.6 x 10^6
OEP	8	4.0 x 10^{11} [c]	4.8 x 10^2	1.2 x 10^{-9}
TAP	2	7.8 x 10^2	1.3 x 10^{10} [b]	1.7 x 10^7
TAP	8	3.7 x 10^{12} [c]	7.9 x 10^3	2.1 x 10^{-9}
TTP	2	6.7 x 10^2	1.3 x 10^{10} [b]	2.0 x 10^7
TTP	8	7.8 x 10^{12} [c]	4.2 x 10^3	5.3 x 10^{-10}
T(p-Cl-P)P	2	8.0 x 10^1	1.3 x 10^{10} [b]	1.7 x 10^8
T(p-Cl-P)P	8	5.0 x 10^{13} [c]	2.6 x 10^4	5.2 x 10^{-10}

[a] Calculated from $K = k_f/k_r$. [b] Diffusion limit, see text. [c] Calculated from Eq.12

parameters found by direct measurement (e.g. $E°'(Ru(THF)^{-1/-2})$), and values found through simulation (e.g. $E°'(RuCl)$) have comparable slopes and R^2 values. Linear behavior is also found

in Hammett plots of the three meso-substituted porphyrins but use of ν(NO) allows direct comparison with the OEP complex.

The loss of chloride from the [Ru(por)(NO)Cl]$^-$ anion becomes more favorable as the porphyrin becomes more electron-donating, as indicated by the increase in log(K_1) with decrease in ν(NO). The R^2 value for this plot is only 0.80, and a closer look at the data suggests that the K_1 for OEP may be overestimated. Since there is clear evidence of the presence of another species in these systems in the CV data, the IR data, and in the VIS-NIR data, some effort was undertaken to explain this discrepancy as discussed below.

The plots of log(K_2), and log(k_{f2}) vs. ν(NO) for the recombination of chloride with the [Ru(por)(NO)(THF)]$^+$ cation (Eq. 7 and Fig. S27) are also linear with R^2 values of 0.99 and 0.95 respectively. The recombination reaction measured by k_{f2} is fastest for the least electron rich species, i.e. the values vary in the order OEP < TAP < TTP < T(*p*-Cl)PP. The rates cover almost two orders of magnitude, i.e. from 4.8 x 10^2 $M^{-1}s^{-1}$ to 2.6 x 10^4 $M^{-1}s^{-1}$. The values of K_2 are also largest for the least electron-donating porphyrin ligand, covering the range of 4 x 10^{11} to 5 x 10^{13}, i.e. 2 orders of magnitude. This order is consistent with the expectation that electrostatic attraction would thermodynamically and kinetically favor chloride recombination with the least electron-rich species.

These reactions are much slower than the diffusion-controlled rate of substitution found for the odd-electron [Ru(por)(NO)Cl]$^-$ species. The [Ru(por)(NO)Cl] starting material is an 18-electron species. Reduction adds one electron (Eq. 1), but bending causes the NO ligand to change from a 3-electron donor to a 1-electron donor (counting all ligands as neutral species). Thus, the [Ru(por)(NO)(Cl)]$^-$ complex is a 17-electron compound. Substitution of a lone pair from a chloride ligand for a lone pair from a THF molecule (Eq. 2) does not change the electron count, which explains why the 17-electron [Ru(por)(NO)(THF)]^0 can be reduced to the 18-electron [Ru(NO)(por)(THF)]$^-$ anion at a potential slightly positive of its precursor chloride complex (Eq. 3). On the other hand, the [Ru(NO)(por)(THF)]$^+$ cation is expected to have a linear NO ligand and thus be an 18-electron species. It has been well established that open-shell species undergo reactions considerably faster than their closed-shell analogues.[38] In this case, comparison of the calculated values of $k_{r2} = K_2/k_{f2}$ with the diffusion limited k_{f1} = 1.34 x 10^{10} M^{-1} s^{-1} suggest that the odd-electron [Ru(NO)(por)Cl]$^-$ anion undergoes THF-for-chloride substitution some *10^{18}-10^{19} times faster* than its neutral [Ru(NO)(por)Cl] precursor!

Second order analysis of [Ru(OEP)(NO)Cl] CV data

From the concentration study by CV, the IR spectroelectrochemistry data, and the VIS-NIR data for the OEP complex, it is clear that the reduction is complicated by a reaction which involves two ruthenium-containing molecules, whose presence is favored by addition of chloride. Further reduction of the [Ru(OEP)(NO)Cl]$^-$ anion itself can be ruled out because its potential is expected to be negative of the [Ru(OEP)(NO)(THF)]^0 feature. Since its calculated structure has a bent NO ligand, its IR band would be expected below 1600 cm^{-1}, rather than the observed 1801 cm^{-1}. The observation of this large band also rules out loss of the NO ligand on the CV timescale, a process discussed recently by Lehnert in the [Fe(TPP)(NO)Cl] system,[11b] although for longer timescales observed in the VIS spectroelectrochemical experiments, significant NO loss seems indicated. However, the EPR data and the VIS data show that significant amounts of the expected [Ru(OEP)(NO)(THF)]^0 form and persist upon reduction of [Ru(OEP)(NO)Cl].

Closer examination of the CV data and the simulations indicate other discrepancies for the OEP complex. The convolved data for the *E°'(RuCl)* and *E°'(Ru(THF)$^{0/-}$)* features show plateaus which are less than one equivalent of electrons in height. Addition of chloride diminishes the intensity of the feature due to *E°'(Ru(THF)$^{+/0}$)* and results in a new peak at E_{pc} = -1.56 V (0.05 V/s). This peak is indicated by the red arrow in Figure S8(B) and S12(B) for OEP and TAP, respectively. These observations suggest a process where [Ru(OEP)(NO)Cl]$^-$ reacts further to make another species. We suggest "dimerization" to make a dimetallic species, to account for the unexpectedly low plateau currents in the convolved data, and the effects observed in the concentration study. The IR band at 1801 cm^{-1} rules out dimerization through the NO ligands, since the expected μ^2-N_2O_2 ligand would be expected to have a ν(NO) band around 1600 cm^{-1}.[39] Dimerization of the [Ru(OEP)(NO)Cl]$^-$ anion is unlikely, as confirmed by DigiElch simulations, because it would have to dimerize faster than the diffusion rate limit to have any effect on the appearance of the CV data. We suggest reaction of the labile, relatively high concentration [Ru(OEP)(NO)(THF] electrode product with the [Ru(OEP)(NO)Cl]$^-$ anion as described by Eq. 14 (where "Ru" = [Ru(OEP)(NO)]) followed by reduction of the thus-formed μ-Cl-dimer (Eq. 15) and rapid decomposition of the dianion (Eq.16), likely with loss of NO, as observed in the VIS spectroelectrochemistry. Given the existence of the [Ru(OEP)]$_2$, which exists with a Ru-Ru bond, steric considerations do not rule out the chloride-bridged dimer species.

$$[Ru(THF)] + [RuCl]^- \leftrightarrows [Ru\text{-}Cl\text{-}Ru]^- + THF \quad (14)$$

$$[Ru\text{-}Cl\text{-}Ru]^- + e^- \leftrightarrows [Ru\text{-}Cl\text{-}Ru]^{2-} \quad (15)$$

$$[Ru\text{-}Cl\text{-}Ru]^{2-} + 3THF \leftrightarrows [Ru(THF)]^- + Cl^- + NO + 2[Ru(OEP)(THF)_2] \quad (16)$$

DigiElch simulations and curve fitting of the CV data where Eq. 14 - 16 are included as supplementary Fig S28. The consideration of these reactions result in better matches to the experimental data in three respects. The first is the diminished charge passed (ca. 0.8 eq) for each of the first two reductions found in the convolved data, i.e. there is less current than expected based on concentration, diffusion coefficient, and other measured parameters. The second improvement is diminishment in the magnitude of the reverse current for the *E°'(Ru(THF)$^{0/-}$)* feature, for which the experimental dimensionless current does not rise above the x-axis. The third feature is that this mechanism better accounts for the diminishment of current for the *E°'(Ru(THF)$^{+/0}$)* feature found when chloride is added. Simulations and curve fitting of the data under scenarios where [Ru(OEP)(NO)(THF)]^0 simply reacted with itself failed to improve these three factors simultaneously. The *K* value for Eq. 14 was

assumed to be large (10^{15}) and the best k_f value was about 2 x 10^9 M^{-1} s^{-1}. For Eq 15, the most-positive E°' value that yielded acceptable results was the same as *E°'(RuCl)* for the OEP complex, with the assumption of a diffusion limited follow-up reaction.

If the charge on the μ-Cl-dimer anion is localized on one RuNO unit, it can be thought of as a neutral [Ru(OEP)(NO)Cl] molecule donating a lone pair from the chloride ligand to the sixth coordination site of a $[Ru(OEP)(NO)]^-$ fragment. This arrangement is consistent with the relative values of *E°'(RuCl)* and *E°'(Ru(THF)$^{0/-}$),* so this charge distribution would result in one linear NO, and one bent NO, consistent with the IR spectroelectrochemical results, but it would be EPR-silent as both metal centers would have 18-electron configurations.

Conclusions

Reduction of the octahedral [Ru(por)(NO)Cl] results in the formation of the neutral [Ru(por)NO)(THF)] species at diffusion limited rates, yet the ligand exchange is a reversible equilibrium process. The reduced complexes have substitutional lability many orders of magnitude greater for the $\{RuNO\}^7$ species than for the $\{RuNO\}^6$ species. The chloride-for-THF metathesis for the odd-electron species is calculated to be some 10^{18} times faster than for the neutral starting material. This result is consistent with the disposition of isolated [Fe(porphyrin)(NO)] complexes to prefer 5-coordinate structures over 6-coordinate structures and indicates that the 6-coordinate ruthenium species may exhibit more similar chemistry to their 5-coordinate iron congeners than might otherwise be expected. This work has demonstrated that very small changes in electron density as measured by the ν(NO) values (e.g. 11 cm^{-1}) translate into order-of-magnitude differences in estimates of rate constants and equilibrium constants.

Experimental Section

General synthetic and electrochemical procedures in these laboratories have been detailed previously.[40] All solvents were pre-dried, distilled, and freeze-pump-thaw degassed before use.[41] Pyrrole, *p*-chlorobenzaldehyde, benzaldehyde, *p*-tolualdehyde, *p*-anisaldehyde were received from Acros, dried with 4Å molecular sieves and distilled before use. NBu_4Cl was used as received from Fischer Chemicals. Ferrocene was obtained from Acros Chemicals, and sublimed before use. Decamethylferrocene was obtained from Johnson-Matthey and used as received. Free base porphyrins[42] and Cp_2CoBF_4[43] were prepared and purified by literature methods. $Ru_3(CO)_{12}$ was used as received from Johnson-Matthey to prepare [Ru(por)CO] complexes.[44] [Ru(por)(NO)Cl] complexes were prepared and purified as described in the literature[14e], with the substitution of the boron trichloride reagent for sequential addition of 1 mL of dry MeOH and two equivalents of acetyl chloride to generate anhydrous HCl. EPR spectra were recorded with a Bruker X-Band EMX^{plus} system equipped with an in-probe liquid-nitrogen Dewar flask for measurements at 77 K. EPR samples were prepared in a drybox under an atmosphere of argon by mixing ~1mL of 1 mM [Ru(OEP)(NO)Cl] in 0.1M NBu_4PF_6/THF with an excess of cobaltocene.

DFT calculations were performed with the Amsterdam Density Functional (ADF2017) program from Scientific Computing and Modeling (SCM; Netherlands).[45-47] The method used was UHF with a TZ2P basis of Slater-type orbitals, and the density functional was GGA:BYLP-D3, with a small frozen core for the lighter atoms and a ZORA relativistic treatment for Ru. The electron density surfaces shown in the figures are plotted at the ADF default value of 0.03 electrons * $(a.u.)^{-3}$.

The geometry optimizations used medium size effective core potentials and the GGA:BLYP XC functional. The spectral calculations (done at the optimized geometries) employed the SOAP[48] model XC potential and used the Davidson Method[49, 50] to determine the low lying excited states and oscillator strengths.

Fiber-optic IR spectroelectrochemistry was performed as previously described.[34] VIS-NIR spectroelectrochemistry was performed in a Pine Instruments spectroelectrochemistry cell with a gold honeycomb working electrode. An Ocean Optics tungsten lamp source, and USB 4000 detector was used for measurements in the 200 – 900 nm region. An Ocean Optics NIR 512 detector was used for measurements in the 900 – 1750 nm region.

All experimental CV data included the internal standard's redox feature, with care to scan the analyte first and the internal standard at the end of each scan. Digital simulations and curve fitting in DigiElch v7F (ElchSoft.com, available from Gamry Instruments, Warminster, PA) were undertaken to extract *E°'* values for Eq. 1, K_1 for Eq. 2, and the k_{f2} values for Eq. 7. A mechanism for each data set was assembled which included the relevant parameters for Eqs. 1-7 (see Results and Discussion), the internal standard, and experimental data. Initial values were entered for all parameters which could be measured from CV data directly. Very fast electron-transfer rates (5 cm^2 s^{-1}) and α = 0.5 were assumed for each electron-transfer reaction. Diffusion coefficients for all Ru-complexes were set at 4 x 10^{-6} cm^2 s^{-1}, decamethylferrocene was used as internal reference[51] and its diffusion coefficient set at 1.2 x 10^{-5} cm^2 s^{-1},[52] and default values from Digisim (i.e. 1 x10^{-5} cm^2 s^{-1})were used for other species. Appropriate concentrations were entered into this mechanism for each species, and simulations were performed with pre-equilibria disabled. The value of k_{f1} was determined to be diffusion-limited (see Results and Discussion), i.e., 1.34 x 10^{10} M^{-1} s^{-1} for THF. A set of 18-24 voltammograms was chosen for each complex at the highest [Ru(por)(NO)Cl] concentration available, and used as a single data set for fitting the simulations to the experimental data. The set used for this study included scans where the (i) switching potential was set just past the first reduction feature, and (ii) scans reversed just past the second reduction feature, each set with 6 scan rates in the range of 0.05 to 1.6 V s^{-1}, with all scans repeated after the addition of ca 10 mM chloride. The values of K_1, *E°(RuCl)*, K_2 and k_{f2} were each refined separately, and then refined together to find the global minimum. Rate constants for reverse reactions are not independent variables and are calculated by DigiElch automatically, i.e. $k_{r1} = K_1/k_{f1}$. Voltammetric data are plotted according to IUPAC convention, with anodic current positive, except where specifically noted in the supplemental material.

Experimental CV data are plotted as dimensionless current vs. potential plots, after correction for iR_u drop and double layer capacitance (see Results and Discussion). LabView 2012 programs were written (MJS) to implement these transformations. DigiElch simulations were performed with values of R_u and C_{dl} estimated from the data, and the curve-fitting process used uncorrected raw data referenced to the $[Cp_2Fe]^{+/0}$ potential. The resulting simulations were corrected in the same way as the experimental data so that trends in the changes of CV shapes could be clearly compared between experiment and simulation. Correction

WILEY-VCH

procedures are discussed in detail in the supplementary information (See Figs. S1-S5, and Tables S1 and S2).

Acknowledgements

We are grateful to the National Science Foundation (CHE-1566509 to GBRA and MJS) for funding for this research.

Keywords: Kinetics • Nitrogen oxides • Nitrosyl • Porphyrinoids • Ruthenium

[1] a) E. G. Abucayon, R. L. Khade, D. R. Powell, Y. Zhang, G. B. Richter-Addo *J. Am. Chem. Soc.* **2016**, 138, 104-107; b) N. Xu, L. E. Goodrich, N. Lehnert, D. R. Powell, G. B. Richter-Addo *Angew. Chem., Int. Ed. Engl.* **2013**, *52*, 3896-3900; c) N. Xu, D. R. Powell, G. B. Richter-Addo *Angew. Chem. Int. Ed Engl.*. **2011**, *50*, 9694-9696; d) S. M. Carter, J. Lee, C. A. Hixson, D. R. Powell, R. W. Wheeler, M. J. Shaw, G. B Richter-Addo, *Dalton Trans*. **2006**, 1338-1346; e) L. Chen, M. A. Khan, G. B. Richter-Addo *Inorg. Chem*. **1998**, *37*, 533-554.

[2] N. Kundakarla, S.Lindeman, M. H. Rahman, M. D. Ryan, *Inorg. Chem.* **2016**, *55*, 2070-2075.

[3] D. P. Linder, K. R. Rodgers, J. Banister, G. R. A. Wyllie, M. K. Ellison, W. R. Scheidt, *J. Am. Chem. Soc*. **2004**, *126*, 14136-14148.

[4] G. R. A. Wyllie, N. J. Silvernail, A. G. Oliver, C. E. Schulz, W. R. Scheidt, *Inorg. Chem*. **2014**, *53*, 3763-3768.

[5] L. E. Goodrich, S. Roy, E. E. Alp, J. Zhao, M. Y. Hu, N. Lehnert, *Inorg. Chem.* **2013**, *52*, 7766-7780.

[6] T. L. Poulos, *Chem. Rev*. **2014**, *114*, 3919-3962.

[7] L. Cheng, G. B. Richter-Addo in *The Porphyrin Handbook*, Vol 4, 219-291 eds R. Guilard, K. Smith, K. M. Kadish, Academic Press, New York: 2000.

[8] J. Yi, A. S. Soares, G. B. Richter-Addo, *Nitric Oxide* **2014**, *39*, 46-50.

[9] J. H. Enemark, R. D. Feltham, *Coord. Chem. Rev*. **1974**, *13*, 339-406.

[10] G. B. Richter-Addo, P. Legzdins, Metal Nitrosyls, Oxford University Press: New York, 1992.

[11] a) N. Xu, D.R. Powell, L. Cheng, G.B. Richter-Addo, *Chem. Commun.* **2006**, 2030-2032; b) A. B. McQuarters, J. W. Kampf, E. E. Alp, M. Hu, J. Zhao N. Lehnert, *Inorg. Chem*. **2017**, *56*, 10513-10528; c) N. Lehnert, W.R. Scheidt, M.W. Wolf, *Struct. Bond*. **2014**, *154*, 155-223; d) G.-B. Yi, L. Chen, M. A. Khan, G. B. Richter-Addo*, Inorg. Chem*. **1997**, *36*, 3876-3885; e) E. G. Abucayon, R. L. Khade, D. R. Powell, M. J. Shaw, Y. Zhang, G. B. Richter-Addo, *Dalton Trans*. **2016**, *45*, 18259-18266; f) G.B. Richter-Addo, R.A. Wheeler, C.A. Hixon, L. Chen, M.A. Khan, M.K. Ellison, C.E. Schulz, W.R. Scheidt, *J. Am. Chem. Soc.* **2001**, *123*, 6314-6326.

[12] P. C. Ford, L. E. Laverman, *Coord. Chem. Rev*. **2005**, 249, 391-403.

[13] F. Doctorovich, D. E. Bikiel, J. Pellegrino, S. A Suárez, M. A. Martí, *Acc. Chem. Res*. **2014**, *47*, 2907–2916.

[14] a) K. M. Kadish, V. A. Adamian, E. V. Caemelbecke, Z. Tan, P. Tagliatesta, P. Bianco, T. Boschi, G.-B. Yi, M. A. Khan, G. B. Richter-Addo, *Inorg. Chem*. **1996**, *35*, 1343-1348; b) D. Awasabisah, N. Xu, K.P.S. Gautam, D.R. Powell, M.J. Shaw, G.B. Richter-Addo, *Dalton Trans*. **2013**, *42*, 8537-8540; c) N. Xu, J. Lilly, D. R. Powell, G. B. Richter-Addo, *Organometallics* **2012**, *31,* 827-834; d) M. A. El-Attar, N. Xu, D. Awasabisah, D. R. Powell, G. B. Richter-Addo, *Polyhedron* **2012**, *40,* 105-109; e) N. Xu, J. Lee, D.R. Powell, G.B. Richter-Addo, *Inorg. Chim. Acta* **2005**, *358*, 2855-2860; f) P. Singh, A. K. Das, B. Sarkar, M. Niemeyer, F. Roncaroli, J. A. Olabe, J. Fiedler, S. Záliš, W. Kaim, *Inorg. Chem.* **2008**, *47*, 7106-7113.

[15] C. Costentin, H. Dridi, J.-M. Savéant, *J. Am. Chem. Soc*. **2014**, *136*, 13727-13734.

[16] I. Bhugun, D. Lexa, J.-M. Savéant, *J. Am. Chem. Soc*. **1996**, *118*, 3982-3983

[17] D. Chong, D. R. Laws, A. Nafady, P. J. Costa, A. L. Rheingold, M. J. Calhorda, W. E. Geiger, *J. Am. Chem. Soc.* **2008** *130*, 2692-2703.

[18] X.-S. Xue, P. Ji, B. Zhou, J.-P. Cheng, *Chem. Rev*. **2017**, *117*, 8622-8648.

[19] K. Bano, A. M. Bond, J. Zhang, *Anal. Chem*. **2015**, *87*, 8387-8393.

[20] a) D. Garreau, J. M. Saveant, *J. Electroanal. Chem*. **1974**, *50*, 1-22; b) L. Nadjo, J. M. Savéant, D. Tessier, *J. Electroanal. Chem*. **1974**, *52*, 403-412.

[21] a) J. M. Savéant, K. B. Su *J. Electroanal. Chem*. **1984**, *171*, 341-349; b) D. J. Martin, B.D. McCarthy, E. S. Rountree, J. L. Dempsey, *Dalton Trans.* **2016**, *45*, 9970-9976.

[22] A. J. Bard, L. R. Faulkner, *Electrochemical Methods: Fundamentals and Applications, Second Edition*, John Wiley and Sons, New York: **2001**.

[23] J.-M. Savéant, *Elements of Molecular and Biomolecular Electrochemistry: An Electrochemical Approach to Electron-Transfer Chemistry*, Wiley-Interscience, Hoboken, New Jersey: 2006, and references therein.

[24] L. Pause, M. Robert, J.-M. Savéant, *J. Am. Chem. Soc*. **2001**, *123*, 11908-11916.

[25] Page 249 of reference 22.

[26] F. Barrière, W. E. Geiger, *J. Am. Chem. Soc.* **2006**, *128*, 3980-3989.

[27] R. S. Nicholson, I. Shain, *Anal. Chem.*, **1964**, *36*, 706–723.

[28] Pages 205-6 of reference 23.

[29] L. Pause, M. Robert, J.-M. Savéant , *J. Am. Chem. Soc.* **2001** *123*, 11908-11916.

[30] Y. Fang, Y. G. Gorbunova, P. Chen, X. Jiang, M. Manowong, A. A. Sinelshchikova, Y. Yu. Enakieva, A. G. Martynov, A. Yu. Tsivadze, A. Bessmertnykh-Lemeune, C. Stern, R. Guilard, K. M. Kadish, *Inorg. Chem.* **2015**, *54*, 3501-3512

[31] N. G. Connelly, W. E. Geiger, *Chem. Rev*. **1996**, *96*, 877–910.

[32] S. Frantz, B. Sarkar, M. Sieger, W. Kaim, F. Roncaroli, J. A. Olabe, S. Zális, *Eur. J. Inorg. Chem*. **2004**, 2902-2907.

[33] (a) S. E. Bari, J. A. Olabe, L. D. Slep, *Adv. Inorg. Chem.* **2015**, *67*, 87-144. (b) W. Kaim, *Inorg. Chem*. **2011**, *50*, 9752-9765.

[34] M. J. Shaw, R. L. Henson, S. E. Houk, J. W. Westhoff, G. B. Richter-Addo, M. W. Jones, *J. Electroanal. Chem*. **2002**, *534*, 47-53.

[35] J. S. Rebouças, B. O. Patrick, B. R. James, *J. Am. Chem. Soc.* **2012**, *134*, 3555-3570.

[36] A. Pacheco, B. R. James, S. J. Rettig, *Inorg. Chem*. **1995**, *34*, 3477-3484.

[37] J. A. S. Roberts, D. L. DuBois, R. M. Bullock *Organometallics* **2011**, *30*, 4555-4563.

[38] R. Poli, *Chem. Rev.* **1996**, *96*, 2135-2204.

[39] Y. Arikawa, T. Asayama, Y. Moriguchi, S. Agari, M. Onishi, *J. Am. Chem. Soc*. **2007**, *129*, 14160-14161.

[40] M. J. Shaw, D. L. Cranford, K. W. Rodgers, J. E. Eilers, B. Noble, A. J. Warhausen, G. B. Richter-Addo, *Inorg. Chem*. **2010**, *49*, 9590 – 9598.

[41] a) D. F. Shriver, M. A. Drezdzon, *The Manipulation of Air-Sensitive Compounds*, 2nd ed.; Wiley-Interscience: Toronto, 1986; b) A. L. Wayda, M. Y. Darensbourg, *Experimental Organometallic Chemistry: A Practicum in Synthesis and Characterization*; American Chemical Society: Washington, D.C., 1987.

[42] A. D. Adler, F. R. Longo, J. D. Finarelli, J. Goldmacher, J. Assour, L. Korsakoff, *J. Org. Chem*. **1967**, *32*, 476-476.

[43] J. E. Sheats, M. D. Rausch , *J. Org. Chem*. **1970** , *35* , 3245-3249.

[44] D.P. Rillema, J.K. Nagle, L.F. Barringer Jr., T.J. Meyer, *J. Am. Chem. Soc*. **1981**, *103*, 56-62.

[45] G. te Velde, F. M. Bickelhaupt, S. J. A. van Gisbergen, C. Fonseca Guerra, E. J. Baerends, J. G. Snijders, T. Zeigler, *J. Comput. Chem*. **2001**, *22*, 931–967.

[46] C. Fonseca Guerra, J. G. Snijders, G. te Velde and E. J. Baerends, *Theor. Chem. Acc.* **1998**, *99*, 391-403.

[47] E. J. Baerends, J. Autschbach, D. Bashford, A. Berces, F. M. Bickelhaupt, C. Bo, P. M. Boerrigter, L. Cavallo, D. P. Chong, L. Deng, R. M. Dickson, D. E. Ellis, M. van Faassen, L. Fan, T. H. Fischer, C. Fonseca Guerra,

A. Ghysels, A. Giammona, S. J. A. van Gisbergen, A. W. Gotz, J. A. Groeneveld, O. V. Gritsenko, M. Gr€uning, F. E. Harris, P. van den Hoek, C. R. Jacob, H. Jacobsen, L. Jensen, G. van Kessel, F. Kootstra, M. V. Krykunov, van E. Lenthe, D. A. McCormack, A. Michalak, M. Mitoraj, J. Neugebauer, V. P. Nicu, L. Noodleman, V. P. Osinga, S. Patchkovskii, P. H. T. Philipsen, D. Post, C. C. Pye, W. Ravenek, J. I. Rodriguez, P. Ros, P. R. T. Schipper, G. Schreckenbach, M. Seth, J. G. Snijders, M. Sola, M. Swart, D. Swerhone, G. te Velde, P. Vernooijs, L. Versluis, L. Visscher, O. Visser, F. Wang, T. A. Wesolowski, E. van Wezenbeek, G. Wiesenekker, S. K. Wolff, T. K. Woo, A. L. Yakolev, T. Ziegler, ADF2017, SCM, *Theoretical Chemistry*, Vrije Universiteit, Amsterdam, The Netherlands, http://www.scm.com, accessed Sept. 16, 2017.

[48] O. V. Gritsenko, P. R. T. Schipper, E. Baerends, *J. Chem. Phys. Lett*. **1999**, *302*, 199–207.

[49] S. J. A. van Gisbergen, J. G. Snijders, E. Baerends, *J. Comput. Phys. Commun.* **1999**, *118*, 119–138.

[50] F. Wang, T. Ziegler, *Mol. Phys*. **2004**, *102*, 2585–2595.

[51] R. Poli, *Chem. Rev.* **1996**, *96*, 2135-2204.

[52] Y. Arikawa, T. Asayama, Y. Moriguchi, S. Agari, M. Onishi, *J. Am. Chem. Soc*. **2007**, *129*, 14160-14161.

WILEY-VCH

Entry for the Table of Contents (Please choose one layout)

Layout 1:

ARTICLE

Irreversible but not inexplicable: Reduction of a series of [Ru(porphyrin)(NO)Cl] results in reversible Cl^- for solvent metathesis at diffusion-limited rates. Cyclic voltammetry, digital simulations IR-, and Vis-spectroelectrochemistry, and EPR studies on a series of complexes reveal equilibrium and rate constants for the reaction shown.

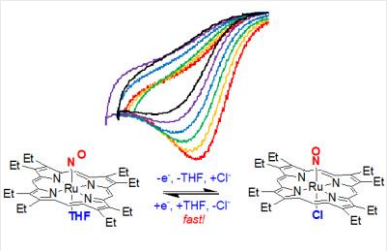

*Jeremy R. Zink, Erwin G. Abucayon, Anthony R. Ramuglia, Arghavan Fadamin, James E. Eilers, George B. Richter-Addo, and Michael J. Shaw**

Page No. – Page No.

Electrochemical investigation of the kinetics of chloride substitution upon reduction of [Ru(porphyrin)(NO)Cl] complexes in THF.

WILEY-VCH